ESKİŞEHİR TEKNİK ÜNİVERSİTESİ BİLİM VE TEKNOLOJİ DERGİSİ B- TEORİK BİLİMLER

Eskişehir Technical University Journal of Science and Technology B- Theoretical Sciences

2023, 11(1), pp. 70-90, DOI: 10.20290/estubtdb.1234016

RESEARCH ARTICLE

DFT CALCULATIONS IN MONOMERIC AND DIMERIC FORMS OF N-BENZYLMALEIMIDE (NBM) COMBINED WITH VIBRATIONAL SPECTROSCOPIC PARAMETERS

Hatice ARI [1,*]

[1] Department of Chemistry, Faculty of Art and Science, Yozgat Bozok University, Yozgat, Turkey

ABSTRACT

The structural, vibrational and theoretical analyses of N-benzylmaleimide (NBM) having chemical and biological significances have been made. The four possible conformers and their sixty-six dimeric forms linked by the intermolecular C=O···H hydrogen bonding were investigated for the stability. The conformational and the dimeric structures of NBM in the gas phase were investigated and the population distributions of the conformations and dimers were obtained using the Boltzmann distribution. The experimental IR and Raman spectra of solid phase NBM were recorded, and the bands were compared with the theoretical wavenumber the values of the monomer and the dimer forms for their assignments. The new scale factors (0.9617 for B3LYP/6-31G(d) and 0.9531 for M06-2X/6-31G(d)) obtained for NBM can be used more accurately in vibration calculations of all maleimide derivatives. The Molecular Electrostatic Potential (MEP) map showed that the negative and the positive regions have changed from monomeric to dimeric form, while the HOMO-LUMO shapes did not generally change in monomeric and dimeric forms. The nucleophilic and electrophilic Fukui functions and dual descriptors shows that maleimide and phenyl groups are nucleophilic and electrophilic attack regions for both forms, respectively, additionally the dual descriptor values decrease upon dimerization.

Keywords: N-benzylmaleimide, Dimer, Scale factor, DFT, Theoretical-vibrational analysis

1. INTRODUCTION

Maleimides and their N-derivatives having bisamide linkages of "-C(=O)-N(R)-C(=O)-" where two carbonyl carbons are linked to a common nitrogen have an important application in organic syntheses [1]. Maleimides are commonly used compounds in bioconjugation due to its excellent chemical reactivity, synthetic accessibility, and practicability as mentioned by Ravasco et al. [2]. This reactive feature of maleimides and their bisamide structures may give rise to interesting reactions like nucleophilic Michael-type addition of thiols or ammines to the vinylene moiety and Diels-Alder reaction with dienes [3]. Maleimides are easily obtained in high yields. They are able to cross biological membranes due to their hydrophobic and neutral nature [4]. Their polymers and N-substituted derivatives are known to show electron withdrawing properties based on a rigid five-membered ring and excellent thermal stability [5]. Maleimide derivatives possess wide range of biological properties such as antimicrobial [1, 6-8], antibacterial [9, 10], antifungal [11, 12], antiviral [13], antitumor [4, 14, 15], antimetastatic [4], antitubercular [16], anti-inflammatory [17], anticancer [18], anxiolytic [19], nematical [20], analgesic [13, 17] and other activities [21].

There is still a great need for development of new maleimide-derived compounds for further investigations employing quantum chemical calculations involving the structural, spectroscopic and electronic properties which will be very useful for those who want to work with these compounds. Therefore, N-benzylmaleimide (NBM) as N-substituted maleimide derivative with the chemical formula $C_9H_9N(CO)_2$, whose molecular structure is given in Figure 1 was employed to examine from electronic,

*Corresponding Author: hatice.ari@bozok.edu.tr
Received: 12.12.2022 Published: 28.02.2023

vibrational spectroscopic and quantum chemical calculations point of view as no such studies have been reported before neither experimental nor theoretical basis.

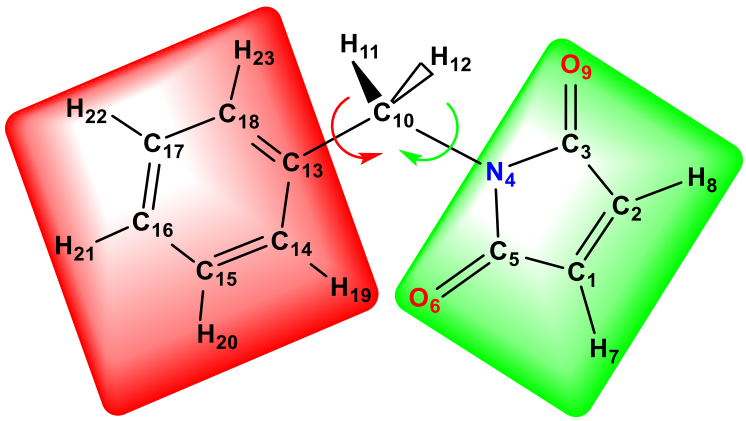

Figure 1. The atom numbering and the flexible rotating dihedral angles of NBM

In the current study, the vibrational spectroscopic and the structural analyses of NBM have been performed. Either the theoretical or the experiment methods were employed to estimate the electronic, the chemical bond and the conformational features of the compound in monomeric and dimeric forms. The following studies were employed on NBM including potential energy surface (PES) scans, MEP, HOMO-LUMO, global reactivity descriptors, local reactivity descriptors (by theoretical methods) and vibrational spectroscopic (experimental & theoretical) analyses using B3LYP and M06-2X functionals with 6-31G(d) basis set in theoretical parts.

2. MATERIALS AND METHODS

Powder crystals of NBM were purchased from Sigma-Aldrich Chemical Company with 99% purity and it was used without any further purification for spectroscopic measurements.

2.1. Vibrational Spectroscopic Details

The Raman measurement of NBM was performed on a Renishaw inVia confocal Raman microscope system at room temperature using 785 nm excitation source of diode laser with 10 sec exposure time. The Leica 50x oil N plan confocal microscopic objective was used to focus the laser beam on the sample. The calibration was made by a silicon standard using the Raman peak centered at 520 cm^{-1}. Nitrogen cooled charge coupled device (CCD) has been used as the detector. Raman spectrum was obtained between 4000-100 cm^{-1} spectral region with a resolution of 0.5 cm^{-1}.

The IR spectrum of NBM was measured in % transmittance mode using Perkin-Elmer Spotlight 400 Spectrometer equipped with Attenuated Total Reflectance (ATR) system having germanium crystal in the 4000-400 cm^{-1} wavenumber region with a resolution of 1 cm^{-1} at room temperature. Tungsten-halogen light source and MCT (mercury cadmium telluride) detector have been used as the additional accessories.

2.2. Computational Details

Gaussian 09W program package [22] (Frisch et al., 2010) were used to perform all the DFT calculations of NBM using different functionals as hybrid-GGA B3LYP [23, 24] and hybrid meta-GGA M06-2X [25] with 6-31G(d) basis set. GaussView 5.0 program [26] were used to visualize the structure and the shapes of the frontier molecular orbitals (FMO), to animate the vibrational frequencies, to draw and examine the MEP surfaces. The Potential Energy Distributions (PED) for each normal mode have been

calculated to obtain contributions of each internal coordinates by the aid of VEDA4 software program package [27]. The optimizations of the dimers were performed along with the counterpoise (CP) correction [28].

3. RESULTS AND DISCUSSION

3.1. Potential Energy Surface (PES) Scan and Conformation Search

NBM, containing phenyl and maleimide rings, has two flexible bonds (shown in Figure 1) and possible conformational isomers can be obtained by the rotations around them. Therefore, to find all possible conformers, the 3D PES scans were performed by varying the torsional angles C_3-N_4-C_{10}-C_{13} (τN_4-C_{10}) and N_4-C_{10}-C_{13}-C_{14} (τC_{10}-C_{13}) in steps 10º between 0º and 360º at B3LYP/6-31G(d) level in vacuum (Figure 2).

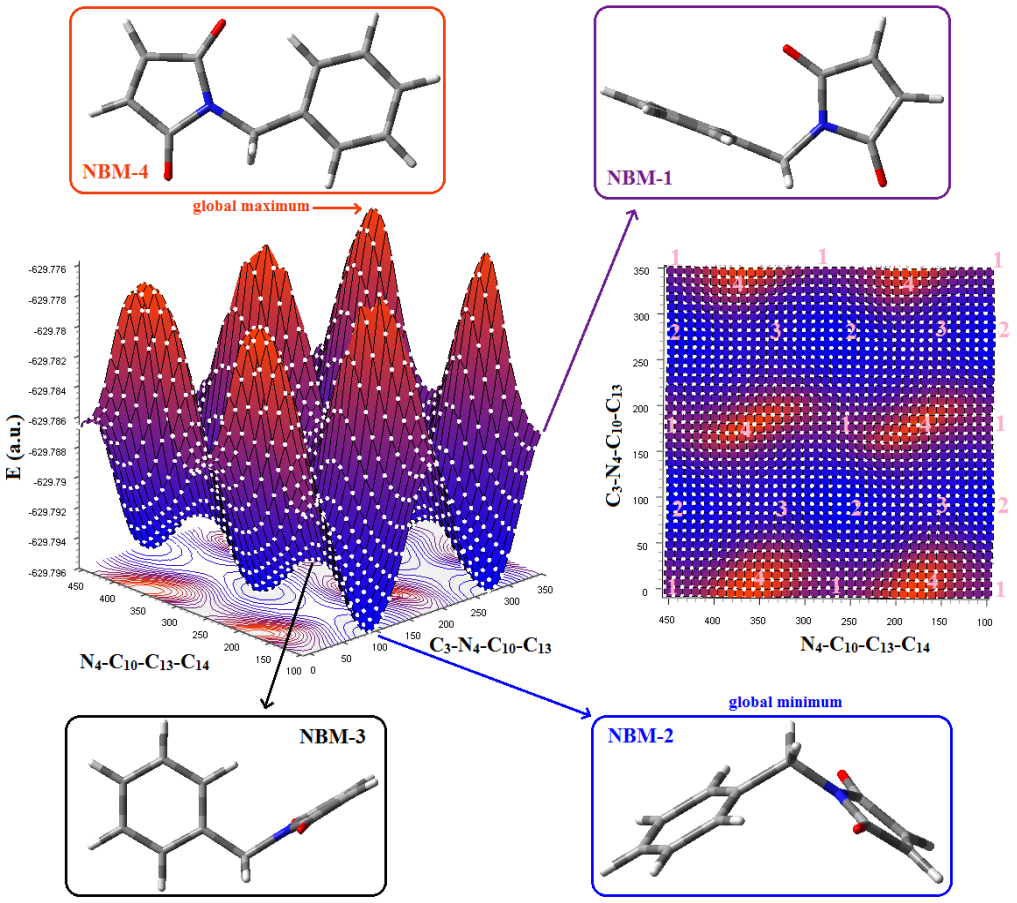

Figure 2. Side (left) and top (right) 3D views of PES curve around the two bonds (B3LYP/6-31G(d)).

Four different structures (NBM-1, NBM-2, NBM-3 and NBM-4) were obtained from the PES graph. In the global maximum structure (NBM-4), both dihedral angles are 0º and both rings are in the same plane. The phenyl and maleimide rings found in NBM-1 and NBM-3 are perpendicular to each other, and the dihedral angles C_3-N_4-C_{10}-C_{13} and N_4-C_{10}-C_{13}-C_{14} are ~180º and ~90º in NBM-1 and ~90º and ~180º in NBM-3, respectively. In the global minimum structure of NBM-2, both dihedral angles are nearly 90º and the conformer has a V-shaped structure due to the positions of the phenyl and maleimide ring planes when we look in the direction of the intersection of these planes. The rotation around the N_4-C_{10} bond requires higher barrier energy than the rotation around the C_{10}-C_{13} bond due to the presence of electronegative O atoms on the maleimide ring and their extra H-bonding effects.

These conformational structures obtained at the highest and the lowest energy levels were re-optimized by B3LYP/6-31G(d) and M06-2X/6-31G(d) levels. The relative energies (ΔE, kcal/mol) and Boltzmann populations (%) of the four conformers were calculated, and given together in Figure 3 for comparison. The energy of the conformer NBM-2 is the lowest as the most stable structure. Its energy is found nearly 2, 6 and 13 kcal/mol lower than that of NBM-3, NBM-1 and NBM-4 conformations, respectively. Consequently, NBM-2 as the most stable conformer with the lowest energy differences (ΔE=0.0 kcal/mol) has the highest populations (97.4%) according to the Boltzmann average.

There are two weak intramolecular H-bonds (2.64Å) in NBN-2 between two carbonyl oxygens of the maleimide ring and bridging methylene hydrogens in addition to two weaker H-bonds between carbonyl oxygens and the two hydrogens of the phenyl ring in para positions (2.94Å). These four H-bonds are most probably the reason for the highest stability of NBM-2 as conformational isomer. The other conformers have no such H-bonding effects as NBM-2.

The dipole moment calculations indicated that NBM-4 was the highest polarity among the other conformers. The order of polarity can be written as μ(NBM-4)> μ(NBM-2)> μ(NBM-3)> μ(NBM-1).

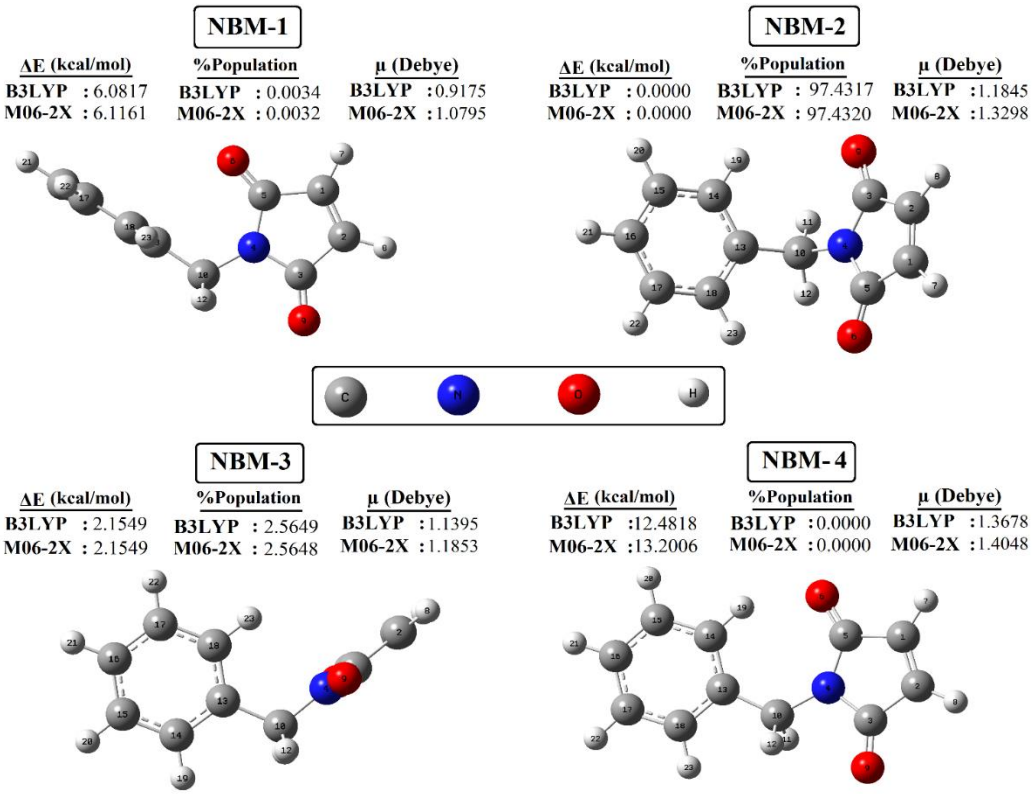

Figure 3. The optimized structures of four stable monomeric conformations of NBM

3.2. Dimeric Structures

The intermolecular hydrogen bonds between the C=O and C-H or C-H_2 groups of both monomeric structures may cause the formation of different NBM dimeric structures. The four different conformational structures obtained gave total of 66 different combinational dimeric structures formed by intermolecular hydrogen bonds. The optimized structures of eight different dimeric structures created from the most stable NBM-2 unit with the highest Boltzmann distribution are given in Figure 4.

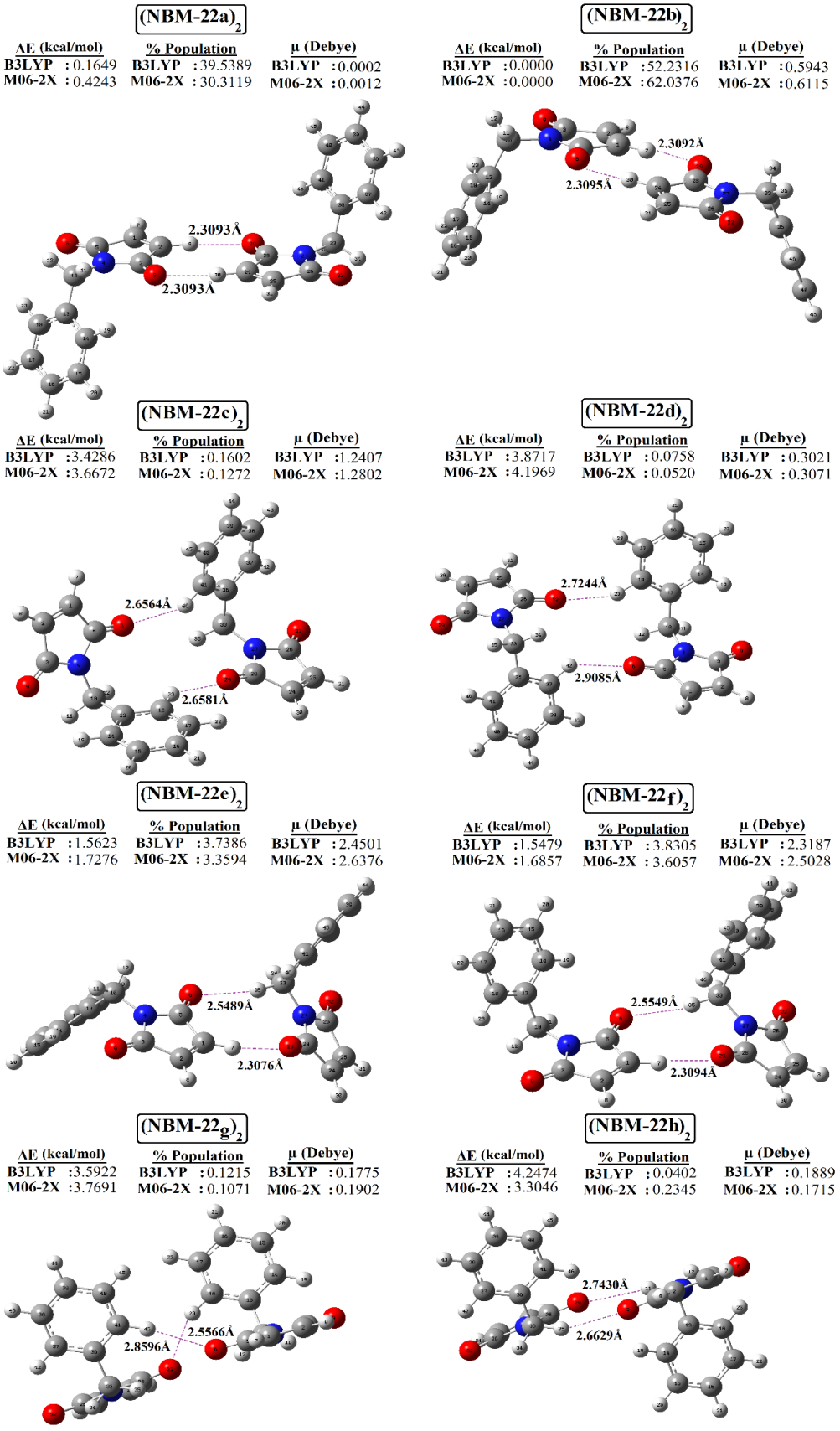

Figure 4. The optimized structures and critical parameters of eight $(NBM\text{-}22)_2$ dimers

Table 1. The relative energies and the populations of 66 dimeric structures

Dimer	Rel. Energy (kcal/mol)		Population (%)	
	B3LYP	**M06-2X**	**B3LYP**	**M06-2X**
$(NBM\text{-}11a)_2$	12.8135	13.0522	0.0000	0.0000
$(NBM\text{-}11b)_2$	12.7832	12.7477	0.0000	0.0000
$(NBM\text{-}11c)_2$	12.8629	13.1161	0.0000	0.0000
$(NBM\text{-}11d)_2$	17.8264	16.4359	0.0000	0.0000
$(NBM\text{-}11e)_2$	16.2496	15.5512	0.0000	0.0000
$(NBM\text{-}11f)_2$	15.2840	15.7181	0.0000	0.0000
$(NBM\text{-}22a)_2$	0.1649	0.4243	39.5389	30.3119
$(NBM\text{-}22b)_2$	0.0000	0.0000	52.2316	62.0376
$(NBM\text{-}22c)_2$	3.4286	3.6672	0.1602	0.1272
$(NBM\text{-}22d)_2$	3.8717	4.1969	0.0758	0.0520
$(NBM\text{-}22e)_2$	1.5623	1.7276	3.7386	3.3594
$(NBM\text{-}22f)_2$	1.5479	1.6857	3.8305	3.6057
$(NBM\text{-}22g)_2$	3.5922	3.7691	0.1215	0.1071
$(NBM\text{-}22h)_2$	4.2474	3.3046	0.0402	0.2345
$(NBM\text{-}33a)_2$	4.8891	4.7465	0.0136	0.0206
$(NBM\text{-}33b)_2$	5.6312	6.0929	0.0039	0.0021
$(NBM\text{-}33c)_2$	9.4063	9.1296	0.0000	0.0000
$(NBM\text{-}33d)_2$	9.4947	9.1589	0.0000	0.0000
$(NBM\text{-}33e)_2$	7.6408	6.3161	0.0001	0.0015
$(NBM\text{-}33f)_2$	7.6488	6.1005	0.0001	0.0021
$(NBM\text{-}44a)_2$	26.0515	27.2640	0.0000	0.0000
$(NBM\text{-}44b)_2$	25.7626	27.1908	0.0000	0.0000
$(NBM\text{-}44c)_2$	29.3146	28.4514	0.0000	0.0000
$(NBM\text{-}44d)_2$	30.1786	30.6303	0.0000	0.0000
$(NBM\text{-}44e)_2$	29.1657	28.9505	0.0000	0.0000
$(NBM\text{-}44f)_2$	31.1575	30.7353	0.0000	0.0000
$(NBM\text{-}12a)_2$	8.0583	8.6081	0.0001	0.0000
$(NBM\text{-}12b)_2$	7.9650	8.6214	0.0001	0.0000
$(NBM\text{-}12c)_2$	10.0681	10.4395	0.0000	0.0000
$(NBM\text{-}12d)_2$	10.3245	9.8877	0.0000	0.0000
$(NBM\text{-}12e)_2$	9.8934	9.8453	0.0000	0.0000
$(NBM\text{-}12f)_2$	9.3229	9.5321	0.0000	0.0000
$(NBM\text{-}12g)_2$	9.3648	10.1666	0.0000	0.0000
$(NBM\text{-}13a)_2$	8.9777	8.9142	0.0000	0.0000
$(NBM\text{-}13b)_2$	9.0823	9.4836	0.0000	0.0000
$(NBM\text{-}13c)_2$	12.7210	12.3487	0.0000	0.0000
$(NBM\text{-}13d)_2$	12.9979	13.2532	0.0000	0.0000
$(NBM\text{-}13e)_2$	11.3026	11.1317	0.0000	0.0000
$(NBM\text{-}13f)_2$	11.9820	12.2352	0.0000	0.0000
$(NBM\text{-}13g)_2$	11.3546	11.4278	0.0000	0.0000
$(NBM\text{-}13h)_2$	11.6992	11.6117	0.0000	0.0000
$(NBM\text{-}14a)_2$	19.6911	20.3168	0.0000	0.0000
$(NBM\text{-}14b)_2$	19.3457	20.5472	0.0000	0.0000
$(NBM\text{-}14c)_2$	22.8425	23.4884	0.0000	0.0000
$(NBM\text{-}14d)_2$	21.3348	22.0242	0.0000	0.0000
$(NBM\text{-}14e)_2$	21.8758	22.7380	0.0000	0.0000
$(NBM\text{-}14f)_2$	21.7485	22.6568	0.0000	0.0000
$(NBM\text{-}14g)_2$	21.0911	22.1247	0.0000	0.0000
$(NBM\text{-}23a)_2$	3.3492	3.8855	0.1832	0.0880
$(NBM\text{-}23b)_2$	4.2368	4.8486	0.0409	0.0173
$(NBM\text{-}23c)_2$	5.5982	5.8116	0.0041	0.0034
$(NBM\text{-}23d)_2$	5.3123	5.3729	0.0067	0.0071
$(NBM\text{-}23e)_2$	6.7011	5.1439	0.0006	0.0105
$(NBM\text{-}23f)_2$	5.1204	5.0750	0.0092	0.0118

Table 1.(Cont.) The relative energies and the populations of 66 dimeric structures

Dimer	Rel. Energy (kcal/mol)		Population (%)	
	B3LYP	**M06-2X**	**B3LYP**	**M06-2X**
$(NBM\text{-}24a)_2$	14.7860	16.2276	0.0000	0.0000
$(NBM\text{-}24b)_2$	14.5323	15.9368	0.0000	0.0000
$(NBM\text{-}24c)_2$	15.9047	15.6390	0.0000	0.0000
$(NBM\text{-}24d)_2$	16.4848	16.1024	0.0000	0.0000
$(NBM\text{-}24e)_2$	15.6612	16.6103	0.0000	0.0000
$(NBM\text{-}24f)_2$	15.7829	17.0805	0.0000	0.0000
$(NBM\text{-}34a)_2$	15.9521	17.2025	0.0000	0.0000
$(NBM\text{-}34b)_2$	16.3013	16.8767	0.0000	0.0000
$(NBM\text{-}34c)_2$	18.1631	18.1050	0.0000	0.0000
$(NBM\text{-}34d)_2$	18.0168	18.2631	0.0000	0.0000
$(NBM\text{-}34e)_2$	15.7742	15.9345	0.0000	0.0000
$(NBM\text{-}34f)_2$	18.0745	17.7641	0.0000	0.0000

Table 1 lists the relative energies and Boltzmann populations of all dimeric structures. It can be seen that $(NBM\text{-}22a)_2$ and $(NBM\text{-}22b)_2$ dimers consisted from the most stable NBM-2 monomers have low relative energies and high populations. The cis $(NBM\text{-}22b)_2$ dimeric configuration where the phenyl groups on the same side of the dimeric plane is more stable than the trans $(NBM\text{-}22a)_2$ dimeric configuration where the phenyl groups on the opposite side of the plane. The two dimeric conformers $(NBM\text{-}22a)_2$ and $(NBM\text{-}22b)_2$ have high stability and the majority of the populations (92% total). The other dimeric conformers have low stabilities and very low populations (8% total). Each NBM-22 dimer has two C=O···H-C intermolecular hydrogen bonds and the shortest (2.31Å) and strongest one found in the $(NBN\text{-}22a)_2$ and $(NBN\text{-}22b)_2$ dimers. The dipole moments of the trans $(NBN\text{-}22a)_2$ and the cis $(NBN\text{-}22b)_2$ dimeric configurations are calculated as 0.0 and 0.6 Debye, respectively.

3.3. Vibrational Characterization

The calculated vibration frequencies of the most stable conformer (NBM-2) and the dimeric forms of this stable structure (the most stable dimer, $(NBM\text{-}22b)_2$ and the second stable dimer, $(NBM\text{-}22a)_2$) by two methods (B3LYP/6-31G(d) and M06-2X/6-31G(d)) were compared with the experimentally measured values of NBM. The vibrational calculations of the monomeric and dimeric forms of NBM were based on the following parameters and assumptions.

The NBM-2 monomer consists of 23 atoms and $\Gamma_{vibration}=34A'+29A''= 63$ vibrational modes with C_s point group symmetry where all the modes are IR and Raman active. The dimeric $(NBM\text{-}22a)_2$ and $(NBM\text{-}22b)_2$ forms on the other hand have 46 atoms having S_2 (C_i) and C_2 point group symmetries, respectively. The dimeric form $(NBM\text{-}22a)_2$ consists of $66A_g+66A_u=132$ vibrational modes ($66A_g$ Raman active, $66A_u$ IR active) in S_2 symmetry and $(NBM\text{-}22b)_2$ form has 67A+65B=132 vibrational modes (both IR and Raman active) in C_2 symmetry.

The tabulated values of the experimental and the calculated (B3LYP) wavenumbers with their potential energy distributions PEDs for NBM-2, $(NBM\text{-}22a)_2$ and $(NBM\text{-}22b)_2$ were listed in Table 2. The force constants $F_c \geq 10\%$ of the contributions are included only in the PED column. The visual comparison of the experimental wavenumbers with the theoretical values of IR and Raman spectral data were presented in Figure 5. The experiments were performed for solid samples while calculations were performed in isolated gas phase; therefore, there are some slight differences between the calculated and the observed vibrational peak intensities rather than wavenumbers.

It can be seen from the table that every experimental value has one corresponding wavenumber in monomeric conformer NBM-2 and two corresponding wavenumbers in the dimeric forms containing two molecules in each dimer. There are extra six low-frequency intermolecular normal vibrations arising

from relative movements of two NBM groups in the dimer. All of these six vibrations are lower in wavenumber values than that of the lowest monomer vibration [29, 30].

Table 2. Experimental and calculated vibrational frequencies (cm^{-1}) with PED and assignments of NBM

Exp. Freq.		Calculated Freq. (B3LYP)			PED (Fc > %10)[a]	Assign.
IR	Raman	NBM-2	$(NBM\text{-}22a)_2$	$(NBM\text{-}22b)_2$		
3159,vw	-	3151	3143, 3143	3144, 3143	99 $K(C\text{-}H)_{mi}$	ν_s CH
3100,vw	3108,vw	3131	3114, 3113	3114, 3113	100 $K(C\text{-}H)_{mi}$	ν_a CH
3091,w	3098,vw	3088	3088, 3088	3088, 3088	98 $K(C\text{-}H)_{ph}$	ν_s CH
3091,vw	3098,vw	3080	3081, 3081	3080, 3080	99 $K(C\text{-}H)_{ph}$	ν_a CH
3069,vw	3073,w	3075	3074, 3074	3074, 3074	98 $K(C\text{-}H)_{ph}$	ν_a CH
3069,vw	3073,w	3067	3066, 3066	3066, 3066	100 $K(C\text{-}H)_{ph}$	ν_a CH
3040,vw	3045,vw	3059	3059, 3059	3059, 3059	99 $K(C\text{-}H)_{ph}$	ν_a CH
2986,vw	2989,vw	3025	3024, 3024	3024, 3024	100 $K(C_{10}\text{-}H)$	ν_a CH_2
2948,vw	2955,vw	2975	2975, 2975	2975, 2975	100 $K(C_{10}\text{-}H)$	ν_s CH_2
1765,w	1768,vs	1781	1778, 1775	1778, 1775	83 $K(C_3{=}O + C_5{=}O)$	ν_s CO
1695,vs	1697,w	1730	1722, 1720	1722, 1720	88 $K(C_3{=}O + C_5{=}O)$	ν_a CO
1606,w	1610,s	1601	1602, 1602	1602, 1602	63 $K(C{=}C)_{ph}$ +25 $H(CCH)_{ph}$	ν CC
1589,w	1592,w	1594	1593, 1593	1593, 1593	87 $K(C{=}C)_{mi}$	ν CC
1579,w	1582,m	1583	1584, 1584	1584, 1584	62 $K(C{=}C)_{ph}$ +16 $H(CCH)_{ph}$+ 12 $H(C_{13}C_{10}H)$	ν CC
1498,w	-	1489	1489, 1489	1489, 1489	64 $H(CCH)_{ph}$ +22 $K(C{=}C)_{ph}$	δ CCH
1458,w	-	1448	1448, 1448	1448, 1448	58 $H(CCH)_{ph}$ +26 $K(C{=}C)_{ph}$	δ CCH
1436,s	1438,m	1444	1445, 1444	1443, 1443	90 $H(HC_{10}H)$	δHCH, sc
1402,s	1406,w	-	-	-	Overtone (700x2)	anh.
1385,m	-	1380	1384, 1384	1383, 1383	52 $H(CC_{10}H)$+25 K(C-N)+20 H(CNC)	δ CCH,wg
1353,s	-	1336	1336, 1336	1338, 1337	61 $H(CC_{10}H)$ +20 $H(CCH)_{ph}$	δ CCH, tw
1340,s	1342,w	1333	1335, 1334	1334, 1333	40 $H(CC_{10}H)$ +18 H(NCH)+11K(C-N)	δ CCH,wg
1310,s	1306,w	1315	1315, 1315	1316, 1316	32 $K(C{=}C)_{ph}$ +23 $H(CCH)_{ph}$	ν CC
1291,w	1294,vw	1289	1296, 1296	1296, 1296	47 $H(CCH)_{mi}$ +15 $K(C\text{-}C)_{mi}$	δ CCH
1291,w	1294,vw	1280	1283, 1281	1283, 1282	44 $H(CCH)_{mi}$ +13 $K(C\text{-}C)_{mi}$+11 $H(CC_{10}H)$	δ CCH
1208,w	1210,s	1185	1185, 1185	1185, 1185	68 $K(C_{13}\text{-}C_{10})$ +15 $H(CCH)_{ph}$	ν CC
1159,m	1161,w	1169	1169, 1169	1170, 1170	82 $H(CCH)_{ph}$ +14 $K(C{=}C)_{ph}$	δ CCH
1137,s	1139,w	1148	1148, 1148	1148, 1148	76 $H(CCH)_{ph}$	δ CCH
1119,sh	1119,s	1119	1122, 1122	1123, 1122	38 $H(CC_{10}H)$+19 K(C-N)+10$K(C\text{-}C)_{mi}$	δ CCH, tw
1109,sh	-	1094	1106, 1104	1106, 1104	55 K(C-N) +24 $H(CCH)_{mi}$	ν CN
1080,m	1084,vw	1073	1075, 1075	1075, 1075	36 $H(CCH)_{ph}$ +15 $K(C{=}C)_{ph}$ +10 $K(C\text{-}C)_{mi}$	δ CCH
1034,m	1035,s	1019	1029, 1029	1029, 1029	64 $K(C{=}C)_{ph}$ +14 $H(CCH)_{ph}$	ν CC
1003,w	1006,vs	1015	1019, 1019	1019, 1019	49 $H(CCH)_{mi}$ +28 K(C-N)	δ CCH
1003,w	1006,vs	1014	1015, 1014	1015, 1014	36 $H(HC_{10}H)$ +15 $K(C\text{-}C)_{mi}$+ 12$H(CCH)_{mi}$	δ HCH, rc
976,vw	-	981	981, 981	981, 981	61 $H(CCC)_{ph}$ +21 $K(C{=}C)_{ph}$+12 $H(CCH)_{ph}$	δ CCC
964,w	961,w	961	962, 961	962, 962	90 $P(C)_{ph}$	γ C
964,w	961,w	937	961, 959	962, 959	96 $P(C)_{ph}$	γ C
929,vw	924,w	928	936, 936	936, 936	98 $P(C)_{mi}$	γ C
918,w	-	903	903, 903	903, 903	81 $P(C)_{ph}$	γ C
880,m	-	865	866, 866	865, 865	45 $H(HC_{10}H)$ +14 H(NCH)	δ HCH, rc
840,s	847,m	832	832, 832	832, 832	97 $P(C)_{ph}$	γ C
815,sh	818,m	813	825, 822	825, 822	66 $P(C)_{mi}$ +10 $P(C)_{ph}$	γ C
781,m	783,w	795	799, 799	799, 799	47 $P(C)_{mi}$ +21 $P(C)_{ph}$	γ C
760,vw	764,w	767	769, 769	768, 768	28 $P(C)_{ph}$ +23 $K(C\text{-}C)_{mi}$	γ C
722,s	731,s	736	737, 737	738, 738	91 $P(C_3{=}O + C_5{=}O)$	γ C
700,sh	705,m	707	708, 708	708, 708	48 $P(C)_{ph}$ +12 $K(C\text{-}C)_{mi}$ +10 K(C-N)	γ C
692,vs	694,sh	688	687, 687	688, 688	88 $P(C)_{ph}$	γ C

Table 2. (Cont.) Exp. and calc. vibrational frequencies (cm^{-1}) with PED and assignments of NBM

Exp. Freq.		Calculated Freq. (B3LYP)			PED (Fc > %10)[a]	Assign.
IR	Raman	NBM-2	$(NBM\text{-}22a)_2$	$(NBM\text{-}22b)_2$		
643,s	646,m	677	677, 675	677, 675	61 $H(CCC)_{mi}$ +21 H(CCN)	δ CCC
623,s	628,s	619	627, 627	628, 627	33 $P(C)_{mi}$ +10 $P(C_3{=}O + C_5{=}O)$	γ C
611,m	619,s	612	611, 611	612, 612	79 $H(CCC)_{ph}$	δ CCC
611,m	619,s	597	605, 604	605, 605	45 $P(C)_{mi}$ +24 $P(C_3{=}O + C_5{=}O)$	γ C
576,s	580,w	562	564, 563	563, 563	61 $H(CCC)_{ph}$	δ CCC
550,vw	-	544	550, 549	550, 549	68 H(CCO) +14 H(NCO) +10	δ CCO
473,vs	481,m	469	470, 470	470, 470	64 $T(CC)_{ph}$	τ CC
405,w	401,w	402	401, 401	401, 401	98 $T(CC)_{ph}$	τ CC
-	-	383	387, 385	387, 385	58 H(NCO)+15 H(CCO)+10 H(CNC)	δ NCO
-	-	339	342, 342	337, 337	59 $T(C_{10}C_{13})$ +20 $T(NC_{10})$	τ CC
-	303,s	288	294, 291	294, 291	97 $T(CC)_{mi}$	τ CC
-	285,m	270	268, 267	273, 272	32 P(N)	γ N
-	215,s	195	201, 200	201, 200	81 $H(C_3NC_{10} + C_5NC_{10})$	δ CNC
-	192,s	170	173, 172	172, 172	84 $T(NC_{10})$ +10 $T(C_{10}C_{13})$	τ CN
-	-	131	137, 131	137, 131	90 $T(CC{+}CN)_{mi}$	τCC+τCN
-	-	52	70, 58	65, 64	51 $T(NC_{10})$ +25 $T(C_{10}C_{13})$	τ CN
-	-	42	54, 51	56, 54	91 $T(CC)_{ph}$	τ CC
-	-	24	51, 41	51, 40	94 $T(CC)_{phenyl}$	τ CC
-	-	-	30, 29	33, 27	-	τ CN (D)
-	-	-	28, 18	25, 17	-	τ CC (D)
-	-	-	11, 9	12, 9	-	τ CC (D)

Note: Intensities of experimental bands are described as; vs: very strong, s: strong, m: medium, w: weak, vw: very weak, sh: shoulder. Groups: ph: phenyl, mi: maleimide, Mode description: s: symmetric, as: asymmetric, υ: stretching (K), δ: in-plane bending (H), γ: out-of-plane bending (P), τ: torsional (T), dimer (D), sc: scissoring, wg: wagging, tw: twisting, rc: rocking, anh: anharmonic vibrations.

The calculated harmonic wavenumbers have been scaled for a better fit with the experimental values due to the basis set insufficiency and vibrational anharmonicity. The new scaling factors 0.9617 and 0.9531 for B3LYP/6-31G(d) and M06-2X/6-31G(d) were obtained by minimizing relative error values, respectively. The scale factor calculations were previously made for these methods by other groups, and the values are given as 0.9613 [31], 0.9614 [32, 33] for B3LYP/6-31G(d) and 0.9496 [34], 0.9463 [35] for M06-2X/6-31G(d), respectively.

The three graphs showing the correlation of the calculated versus the experimental wave numbers of the conformers NBM-2, $(NBM\text{-}22a)_2$ and $(NBM\text{-}22b)_2$ by B3LYP/6-31G(d) and M06-2X/6-31G(d) and their % relative errors (Figure 6) compare these methods to decide the best. The percent relative errors for the methods B3LYP/6-31G(d) and M06-2X/6-31G(d) were found to be 0.97% and 1.20% for NBM-2, 0.87% and 1.24% for $(NBM\text{-}22a)_2$ and 0.87% and 1.18% for $(NBM\text{-}22b)_2$, respectively. The lowest percent relative error values were obtained for the dimeric structure $(NBM\text{-}22b)_2$ in the calculations by the two methods for monomeric and dimeric forms. The % relative errors obtained by B3LYP are lower than those obtained by M06-2X in the calculations for all structures. The R-squared (R^2) values are higher in B3LYP than in M06-2X for all the structures. The R^2 values are higher for the dimers than that for the monomers in all the methods. The best linear correlation has been obtained with the calculation of B3LYP/6-31G(d) for $(NBM\text{-}22b)_2$ where $y = 1.0024x\text{-}0.9207$ with $R^2 = 0.9998$ where the slope and intersection values are much closer to 1 and 0, respectively. Therefore, only the frequency values calculated by the B3LYP/6-31G(d) basis set gives the closest result to the experimental values (Table 2) among all the vibrational wavenumbers calculated for the three structures.

The NBM molecule consists of phenyl and maleimide rings combined with a methylene group, so the definition of characteristic vibrational modes is divided into the following two headings: (i) phenyl and (ii) maleimide rings for simplicity.

3.3.1. Maleimide ring vibrations

Woldbaek et al. noted that the symmetric and asymmetric C-H stretching vibrations were observed at 3104 cm^{-1} and 3170 cm^{-1}, respectively [36]. For the same C-H stretching vibrations of NBM symmetric one (ν_s CH) occurred at 3159 cm^{-1} and asymmetric one (ν_a CH) at 3100 cm^{-1}. The symmetric C=O stretching vibrations appeared at 1765 cm^{-1} as weak band in IR and at 1768 cm^{-1} as very intense band in Raman while the asymmetric C=O stretching vibration occurred at 1695 cm^{-1} as very intense band in IR and at 1697 cm^{-1} as weak band in Raman. The C=C stretching vibration of the maleimide ring occurred at 1589 (IR) and 1592 (Raman) cm^{-1} as weak bands.

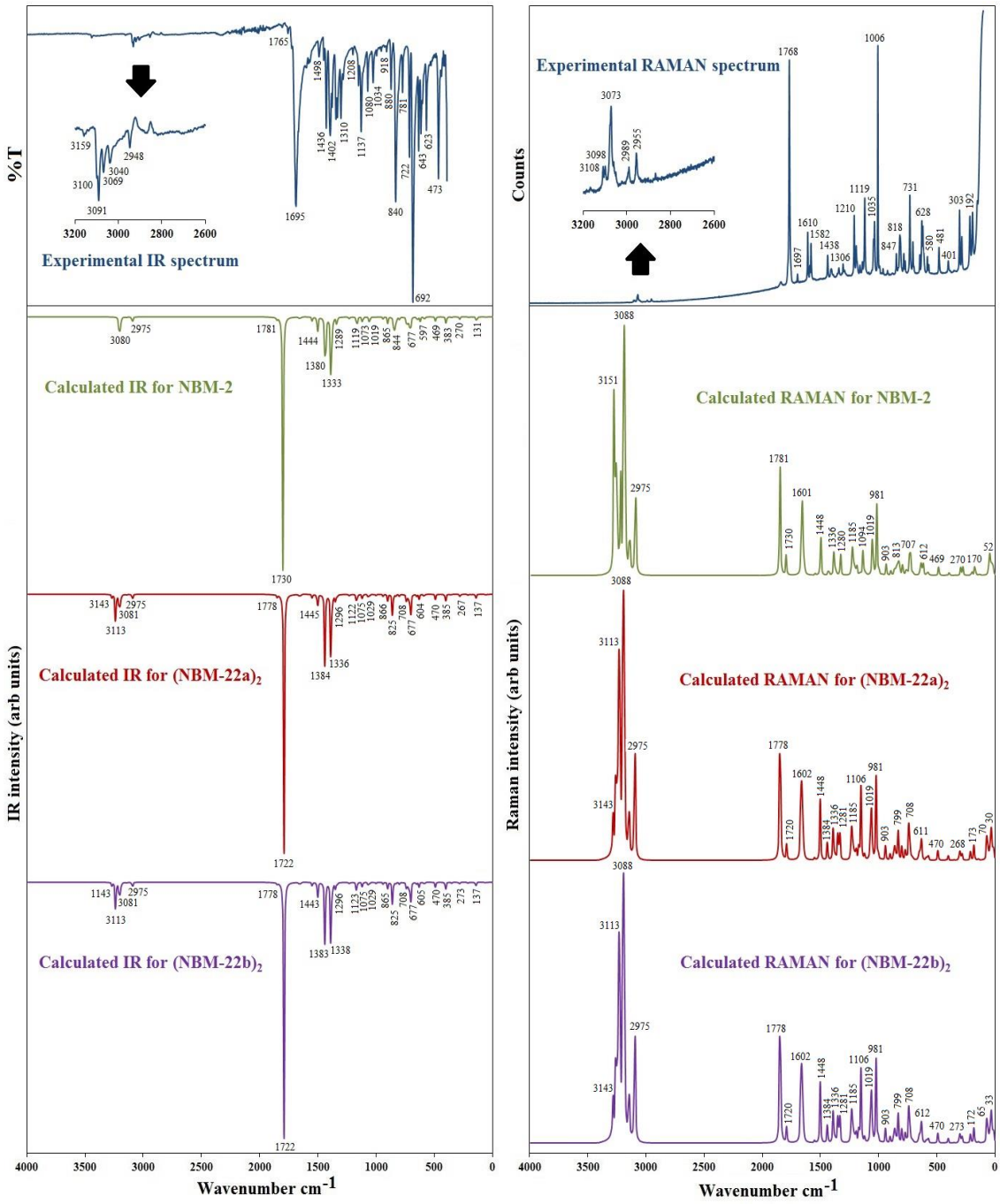

Figure 5. The experimental (upper) and the calculated (B3LYP) IR and Raman spectra of NBM in monomeric and dimeric forms (lower).

3.3.2. Phenyl ring vibrations

In general, aromatic C-H stretching vibrations appears above 3000 cm^{-1} in the spectrum [37]. In this study, the IR bands appeared in the range 3091-3040 cm^{-1} and the Raman bands appeared in 3098-3045 cm^{-1} range regarding NBM molecule were all assigned to C-H stretching vibrations of phenyl ring with 98-100% contributions in the PED table of their calculated wavenumbers. The C=C stretching vibrations of aromatic rings along with the CCH in-plane bending modes were observed at 1606, 1579, 1498, 1458, 1310, 1159, 1080, 1034 and 976 cm^{-1}. The CH_2 group bands are mainly grouped into six fundamental vibrations namely CH_2 symmetric and CH_2 asymmetric stretchings, CH_2 scissoring and CH_2 rocking as in plane bendings and CH_2 wagging and CH_2 twisting as out of plane bendings [38]. The energies of these CH_2 in-plane and out-of-plane vibrational modes mostly follow the following order; CH_2 sciss > CH_2 wag > CH_2 twist > CH_2 rock [39] and observed generally in the 1500-800 cm^{-1} region [40]. In this study, the bands at 2986 cm^{-1} (IR) and 2989 cm^{-1} (Raman) were assigned to asymmetrical stretching, while the bands at 2948 cm^{-1} (IR) and 2955 cm^{-1} (Raman) were assigned to symmetrical stretching of methylene groups (CH_2). The bands at 1436 cm^{-1} (IR, s) and 1438 cm^{-1} (Raman, m) were predicted to be the CH_2 scissoring modes. The bands observed at 1385 and 1340 cm^{-1} (IR) and 1342 cm^{-1} (Raman) were assigned to the CH_2 wagging modes. The bands at 1353, 1119 cm^{-1} and 1003, 880 cm^{-1} were assigned to the CH_2 twisting and CH_2 rocking modes, respectively.

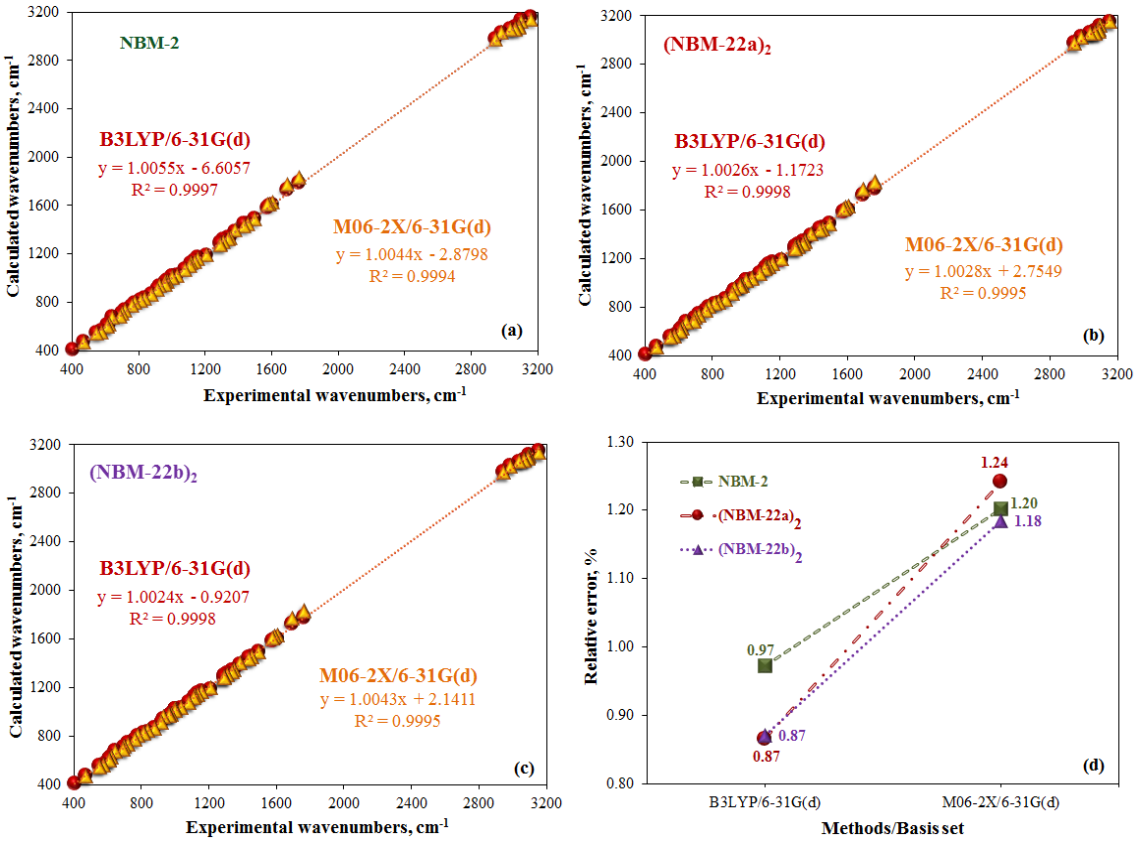

Figure 6. The comparison of the correlation graphics for the experimental wavenumbers vs the calculated wavenumbers with their R^2 values (a-c) and for the % relative errors vs. the methods for the monomeric and the dimeric structures of NBM (d).

3.4. Molecular Electrostatic Potential (MEP) Analysis

The MEP plot gives information of electrostatic potential as mapped onto the constant electron density surface and still a good guide in assessing the molecular reactivity against positively or negatively

charged reactive species. The maximum negative regions were mostly indicated as red color for electrophilic attack regions while the maximum positive regions were marked as blue color for nucleophilic attack sites in the MEP and contour maps as a general tendency.

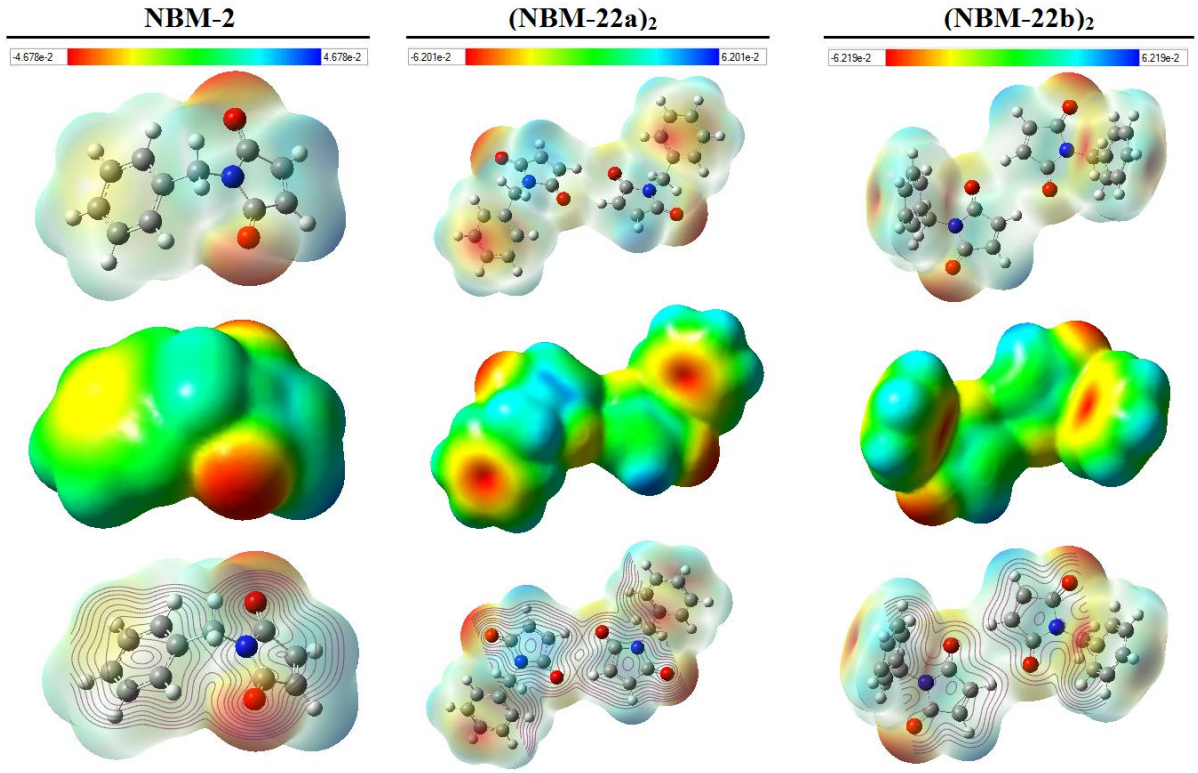

Figure 7. The MEP and contour maps for the monomeric and the dimeric forms of NBM.

The MEPs of NBM in monomeric and dimeric forms were visualized as the result of the calculation by the method B3LYP/6-31G(d) as given in Figure 7 with their color grading for comparison. The limit of molecular electrostatic potential is ±0.04678 a.u. in the monomeric structure, while it is ±0.06201 a.u. for $(NBM\text{-}22a)_2$) and ±0.06219 a.u. for $(NBM\text{-}22b)_2$ in the dimeric structures. Further examination of the MEP map of the NBM-2 conformer, it is can be seen that the electron-rich red regions are over the electronegative oxygen atoms, and the more electron-deficient navy-blue regions are over the hydrogen atoms in the both maleimide ring. When the MEP maps of the dimeric structures are examined, it can be seen that the same oxygens are yellow in color and the same hydrogens are light blue in color due to the C=O···H-C intermolecular interactions. The oxygen atoms and the hydrogen atoms of the maleimide ring that are not involved in intermolecular hydrogen bonding upon dimerization are still electron-rich red regions and electron-deficient dark blue regions, respectively. The red colored electron rich region can only be observed on carbonyl oxygens in the monomeric form but it can be observed both over benzene ring and on non-H-bonded carbonyl oxygens in dimeric forms indicating that the electrophilicity property is shifted partly to the benzene ring upon dimerization because of H bonding effect.

3.5. HOMO-LUMO Analysis

The energy difference between LUMO (Lowest Unoccupied Molecular Orbital), and HOMO (Highest Occupied Molecular Orbital) is called the HOMO-LUMO gap (ΔE_{gap}) which is a measure of electron conductivity and helps characterize molecular reactivity and kinetic stability [41].

The ΔE_{gap} value of NBM were calculated as 4.10 eV, 4.12 eV and 4.13 eV at B3LYP/6-31G(d) (Table 3). This shows that the molecular reactivity decreases and it is kinetically stabilized when NBM dimerizes. 3D plots of HOMO-LUMO shapes helps us to visualize positive and negative charge accumulations on the molecular orbital surfaces (Figure 8). The most stable conformer and the two dimeric forms of the NBM compound shown in this figure can be analyzed easily. The red colored lobes represent positive charges and green lobes represent negative charges. HOMO and LUMO are the main orbitals involved in chemical reactions and the HOMO-1 and the LUMO+1 orbitals represent the corresponding donor and the acceptor energy levels, which are below and above these energy levels, respectively. In NBM-2, HOMO is mainly localized on the phenyl ring, while LUMO is mainly localized on the maleimide ring. Like the HOMO and HOMO-1 shapes, the LUMO and LUMO+1 shapes are quite different from each other in NBM-2. No difference is observed between them in dimeric structures. It is clear that HOMOs and LUMOs of dimeric structures are mainly localized on maleimide rings.

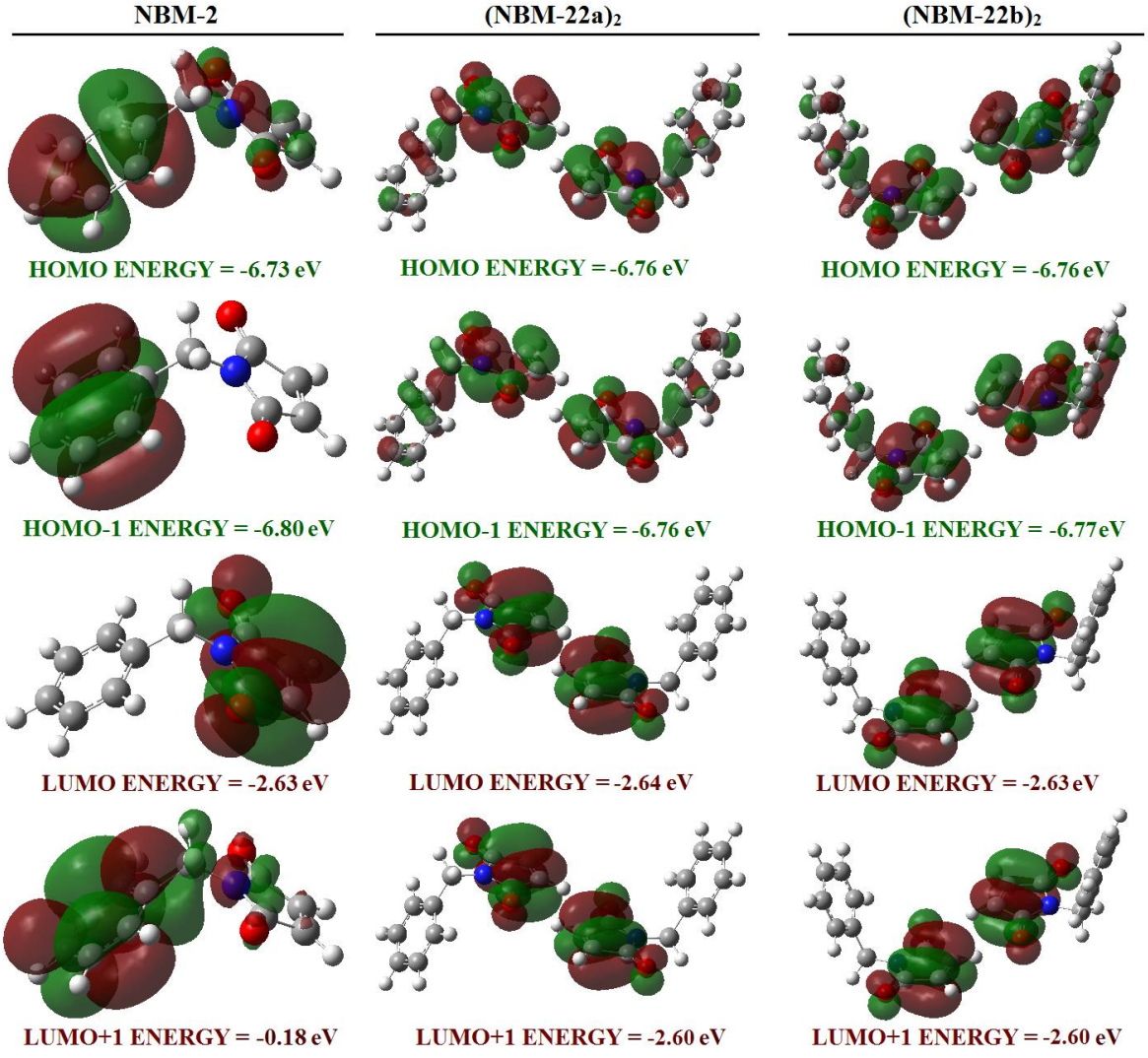

Figure 8. 3D HOMO-LUMO plots for the monomeric and the dimeric structures of NBM.

3.6. Global Reactivity Descriptors

Global reactivity descriptors, including ionization potential (IP), electron affinity (EA), electronegativity (χ), chemical potential (μ), chemical hardness (η), global softness (S), electrophilic index (ω), maximum

charge transfer index (ΔN_{max}), nucleofugality (ΔE_n), electrofugality (ΔE_e) and back donation ($\Delta E_{back\text{-}donation}$) can be calculated using HOMO & LUMO orbital energies as suggested in Koopman's theorem [42, 43] to achieve the reactivity properties of molecules.

Table 3. HOMO & LUMO energies and global reactivity descriptors of NBM (eV)

Parameters	NBM-2		$(NBM\text{-}22a)_2$		$(NBM\text{-}22b)_2$	
	B3LYP	**M06-2X**	**B3LYP**	**M06-2X**	**B3LYP**	**M06-2X**
HOMO Energy (E_{HOMO})	-6.7267	-8.1333	-6.7599	-8.1782	-6.7629	-8.1801
LUMO Energy (E_{LUMO})	-2.6286	-1.5146	-2.6403	-1.5287	-2.6349	-1.5268
HOMO-LUMO Energy Gap (ΔE_{gap})	4.0981	6.6187	4.1196	6.6494	4.1280	6.6532
Ionization Potential ($IP = -E_{HOMO}$)	6.7267	8.1333	6.7599	8.1782	6.7629	8.1801
Electron Affinity ($EA = -E_{LUMO}$)	2.6286	1.5146	2.6403	1.5287	2.6349	1.5268
Electronegativity ($\chi = (IP+EA)/2$)	4.6777	4.8239	4.7001	4.8535	4.6989	4.8535
Chemical Potential ($\mu = -(IP+EA)/2$)	-4.6777	-4.8239	-4.7001	-4.8535	-4.6989	-4.8535
Chemical Hardness ($\eta = (IP-EA)/2$)	2.0490	3.3093	2.0598	3.3247	2.0640	3.3266
Global Softness ($S = 1/2\eta$)	0.2440	0.1511	0.2427	0.1504	0.2422	0.1503
Electrophilicity Index ($\omega = \mu^2/2\eta$)	5.3393	3.5159	5.3625	3.5426	5.3488	3.5405
Charge transfer ($\Delta N_{max} = -\mu/\eta$)	2.2829	1.4577	2.2819	1.4598	2.2766	1.4590
Nucleofugality ($\Delta E_n = (\mu+\eta)^2/2\eta$)	7.9679	5.0305	8.0028	5.0713	7.9837	5.0674
Electrofugality ($\Delta E_e = (\mu-\eta)^2/2\eta$)	12.0660	11.6491	12.1224	11.7207	12.1117	11.7206
Back donation ($\Delta E_{back\text{-}donation} = -\eta/4$)	-0.5123	-0.8273	-0.5149	-0.8312	-0.5160	-0.8317

If we examine the values of HOMO & LUMO and global reactivity descriptors calculated by the two methods for NBM forms given in Table 3, it is seen that the most stable dimeric structure ($(NBM\text{-}22b)_2$) has the highest ΔE_{gap}, IP, and η values, while the other dimeric structure ($(NBM\text{-}22a)_2$) as the second most stabile dimeric form has the highest EA, χ, ω, ΔE_n and ΔE_e values. The most stable monomeric form (NBM-2) has the highest μ, S, ΔN_{max} and $\Delta E_{back\text{-}donation}$ values. The electrophilicity index (ω) classifies the organic compounds as strong electrophiles with $\omega > 1.5$ eV, moderate electrophiles between $0.8 < \omega < 1.5$ eV, and very weak electrophiles between $\omega < 0.8$ eV [44]. Parthasarathi et al. showed that there could be a reliable relationship between the electrophilic index and various biological activities and that electrophilicity can be used as a descriptor of biological activity [45]. Here, the calculation results showed that ω values of all the monomeric and the dimeric forms of NBM are said to be a good electrophile and have biological activities with higher ω values above 1.5 eV.

3.7. Fukui Functions and Dual Reactivity Descriptors

Yang et al. developed a condensed Fukui function as a local reactivity descriptor to determine the reactivity of each center in a molecule [46-48]. The condensed Fukui functions can help to define the reactivity feature of each atom as electrophile and nucleophile. This is accomplished by the analysis of electron population in two ways either by using natural population analysis (NPA) or Mulliken Population Analysis (MPA). The latter is used more commonly in analyses. Independent calculations for a system of N electrons are performed which correspond to cationic (N-1); neutral (N) and anionic (N+1) electronic states keeping the same molecular geometry. For each atom of a molecule condensed Fukui functions are used by the following equations;

$$f^+(r) = [N_k(N) - N_k(N+1)]$$
$$f^-(r) = [N_k(N-1) - N_k(N)]$$

where N_k is the electronic population on atom k in a system. From the calculated values of $f^+(r)$ and $f^-(r)$ one can decide that a center is susceptible to electrophilic attack when the values of $f^+(r)$ are large and positive while nucleophilic attack site has large and positive $f^-(r)$ is value.

Another local reactivity indicator can be used as derivative of the Fukui function with respect to electron number that was defined as dual descriptor [49]. The dual descriptor is known to be more efficient than the proper Fukui function to predict the reactive sites of on a molecule [50, 51]. The dual descriptors are also defined by Barluenga et al as the difference between Fukui functions where the values of them are related to electron density of the frontier orbitals [52].

$$\Delta f(r) = f^{+}(r) - f^{-}(r) \approx \rho^{LUMO}(r) - \rho^{HOMO}(r)$$

From this equation the site is favored for a nucleophilic attack if $\Delta f(r)>0$, whereas the site is favored for an electrophilic attack if $\Delta f(r)<0$ [49, 53].

The condensed Fukui functions and the dual reactivity descriptors calculated for NBM-2, $(NBM\text{-}22a)_2$ and $(NBM\text{-}22b)_2$ are tabulated in Table 4 and the dual reactivity descriptors for the nucleophilic and the electrophilic attack centers of NBM are shown in Figure 9.

Table 4. Condensed Fukui functions and dual reactivity descriptors of NBM

Atom	NBM-2			$(NBM\text{-}22a)_2$			$(NBM\text{-}22b)_2$		
	$f^{+}(r)$	$f^{-}(r)$	$\Delta f(r)$	$f^{+}(r)$	$f^{-}(r)$	$\Delta f(r)$	$f^{+}(r)$	$f^{-}(r)$	$\Delta f(r)$
C_1	0.1458	0.0320	0.1138	0.0818	0.0122	0.0696	0.0603	0.0082	0.0520
C_2	0.1457	0.0324	0.1134	0.0603	-0.0019	0.0622	0.0815	0.0160	0.0656
C_3	0.0886	-0.0103	0.0989	0.0508	0.0020	0.0488	0.0458	-0.0029	0.0487
N_4	0.0080	0.0745	-0.0665	0.0076	-0.0025	0.0101	0.0076	0.0179	-0.0103
C_5	0.0885	-0.0102	0.0988	0.0454	0.0002	0.0452	0.0507	-0.0022	0.0529
O_6	0.1582	0.0544	0.1038	0.0941	0.0211	0.0730	0.0636	0.0149	0.0487
O_9	0.1582	0.0538	0.1044	0.0637	0.0046	0.0591	0.0944	0.0292	0.0652
C_{10}	-0.0065	-0.0299	0.0234	-0.0041	-0.0066	0.0026	-0.0044	-0.0175	0.0131
C_{13}	-0.0347	0.1723	-0.2069	-0.0208	-0.0079	-0.0129	-0.0207	0.1120	-0.1327
C_{14}	-0.0018	0.0403	-0.0421	-0.0034	0.0795	-0.0829	-0.0028	0.0154	-0.0182
C_{15}	0.0126	0.0318	-0.0191	0.0063	0.0765	-0.0703	0.0062	0.0259	-0.0196
C_{16}	0.0239	0.1859	-0.1620	0.0149	-0.0112	0.0260	0.0147	0.1143	-0.0997
C_{17}	0.0126	0.0318	-0.0191	0.0091	0.0842	-0.0751	0.0088	0.0135	-0.0047
C_{18}	-0.0018	0.0403	-0.0421	0.0006	0.0759	-0.0754	-0.0005	0.0298	-0.0303
C_{24}				0.0603	0.0058	0.0546	0.0603	-0.0025	0.0628
C_{25}				0.0818	0.0172	0.0646	0.0815	0.0116	0.0700
C_{26}				0.0454	-0.0030	0.0484	0.0458	-0.0005	0.0462
N_{27}				0.0076	0.0151	-0.0075	0.0076	-0.0026	0.0102
C_{28}				0.0508	-0.0012	0.0520	0.0507	0.0015	0.0492
O_{29}				0.0637	0.0161	0.0476	0.0636	0.0030	0.0606
O_{32}				0.0941	0.0243	0.0698	0.0944	0.0169	0.0775
C_{33}				-0.0041	-0.0171	0.0130	-0.0044	-0.0071	0.0027
C_{36}				-0.0208	0.1129	-0.1337	-0.0207	-0.0064	-0.0143
C_{37}				0.0006	0.0218	-0.0212	-0.0028	0.0841	-0.0868
C_{38}				0.0091	0.0219	-0.0128	0.0062	0.0718	-0.0655
C_{39}				0.0149	0.1159	-0.1010	0.0147	-0.0117	0.0264
C_{40}				0.0063	0.0179	-0.0117	0.0088	0.0889	-0.0801
C_{41}				-0.0034	0.0231	-0.0266	-0.0005	0.0724	-0.0729

The most reactive site of NBM-2 for nucleophilic attacks is the double bonded carbon atoms in the maleimide ring (C_1=C_2 > O_6 & O_9 > C_3 & C_5) whereas the important reactive sites for electrophilic attacks are the carbons in the para, ortho and meta positions of the phenyl ring, respectively (C_{13} > C_{16} > C_{14} & C_{18} > C_{15} & C_{17}). From the dual reactivity descriptor values, the nucleophilic spots (centers) are in maleimide ring can be ordered as (O_6 > O_{32} > C_1 > C_{25} > C_2 > O_9 > C_{24} > C_{28} > C_3 > C_{26} > O_{29} > C_5) while the electrophilic spots (centers) are mainly ordered in benzene ring as (C_{36} > C_{39} > C_{14} > C_{18} > C_{17}

> C_{15} > C_{41} > C_{37} > C_{13} > C_{38} > C_{40}) for $(NBM\text{-}22a)_2$. For the $(NBM\text{-}22b)_2$ dimeric structure, the nucleophilic and electrophilic points are located same as the other dimer on maleimide and benzene rings, respectively. They are ordered with respect to their Δf(r) values as; O_{32} > C_{25} > C_2 > O_9 > C_{24} > O_{29} > C_5 > C_1 > C_{28} > C_3 > O_6 > C_{26} for the nucleophilic and C_{13} > C_{16} > C_{37} > C_{40} > C_{41} > C_{38} > C_{18} > C_{15} > C_{14} > C_{36} > C_{17} for the electrophilic characters.

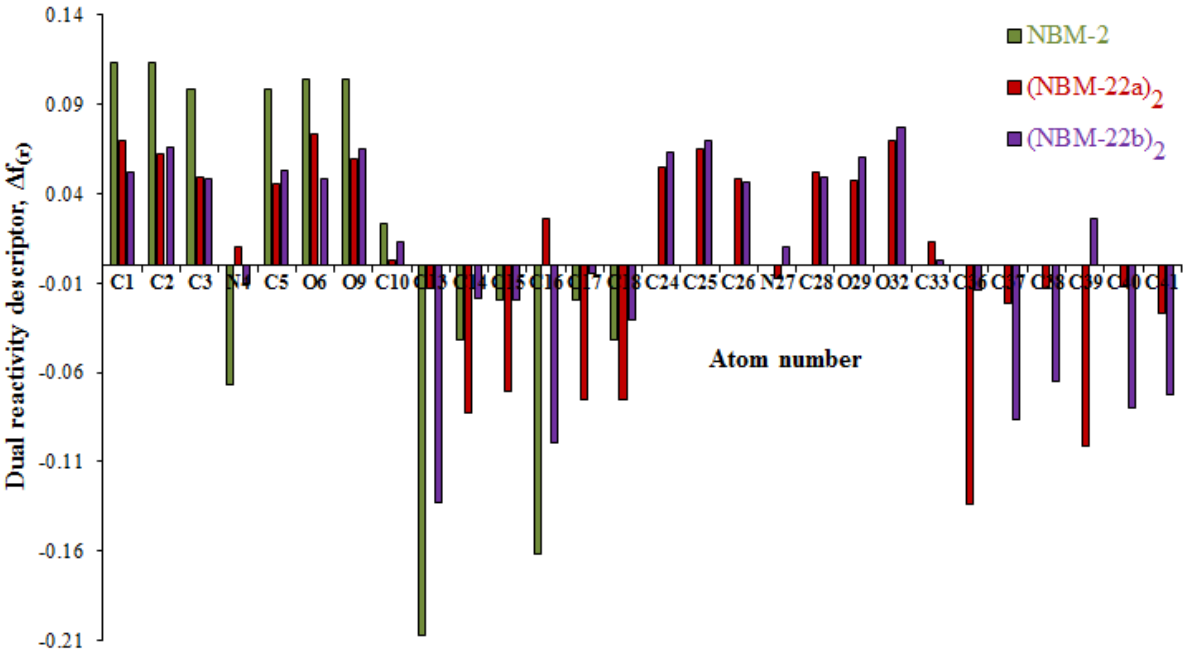

Figure 9. The dual reactivity descriptors of NBM forms calculated at B3LYP/6-31G(d).

4. CONCLUSION

The four conformers with relative energy intervals between 0 and 13 kcal/mol and all having C_s point group symmetry were found as a result of the PES scans. The order of stability in the monomeric conformers can be given as NBM-2 > NBM-3 > NBM-1> NBM-4. The 66 dimeric structures were formed over 10 different binding ways of all conformers found. The order of stability for the dimers was obtained as; $(NBM\text{-}22)_2$ > $(NBM\text{-}23)_2$ >$(NBM\text{-}33)_2$ > $(NBM\text{-}12)_2$ > $(NBM\text{-}13)_2$ > $(NBM\text{-}11)_2$ > $(NBM\text{-}24)_2$ > $(NBM\text{-}34)_2$ > $(NBM\text{-}14)_2$ >$(NBM\text{-}44)_2$. Among all these forms, the homo-dimeric structures ($(NBM\text{-}22)_2$) of the most stable monomeric conformer (NBM-2) is much more stable than the others.

The comparison of calculated wavenumbers with the experimental analogous showed that the lowest % relative error has been obtained for $(NBM\text{-}22b)_2$ calculated by B3LYP/6-31G(d). These results favor the dimeric structure in the solid state of NBM and support the fact that B3LYP/6-31G(d) regenerate the experimental data better than the others.

The MEP map shows that the potential negative and positive sites changes in monomeric and dimeric forms. In the monomeric form, the electron-rich red regions and the electron-deficient dark blue regions are located over two electronegative oxygen atoms and two hydrogen atoms in the maleimide ring, respectively. These regions change by dimerization, in such a way that the oxygens and hydrogens included in the H-bonding in the dimers, lose their electron-rich and electron-deficient characters, while new nucleophilic and electrophilic attack regions are formed. The new electrophilic center appears partly over the benzene ring in addition to non-H-bonding oxygen of the maleimide carbonyl of the dimer. The nucleophilic centers are mainly located on maleimide ring hydrogens in monomeric NBM but in dimeric forms although the non-H-bonding hydrogens of the maleimide ring keep their nucleophilic characters

there is a partly shift to phenyl hydrogens especially in para positions of the dimeric structures as shown by electron-deficient dark blue regions.

The HOMO-LUMO band gap values calculated by both methods showed that the most stable dimeric structure has the largest HOMO-LUMO gap of 0.03 eV than the others, so it is less reactive than the others and is associated with high kinetic stability indicating that one is the hard molecule. The calculated high electrophilicity index values of NBM indicate that it is a good electrophile and has useful biological activity.

Condensed Fukui functions and dual reactivity descriptor data indicate that the most desirable site for electrophilic attack is observed at C_{13} (in the phenyl ring) and that for nucleophilic attack is found at C_1=C_2 (in the maleimide ring) of NBM monomer. In $(NBM\text{-}22a)_2$ and $(NBM\text{-}22b)_2$, dimers, the most important site for nucleophilic attack is O_6 or O_9 (at the maleimide ring), which do not participate in dimerization, while C_{13} (on the phenyl ring bridging C) keeps its electrophilic attack site feature. The $\Delta f(r)$ values of the NBM-2 monomer are higher than that of the dimers confirming its highest reactivity.

CONFLICT OF INTEREST

The author stated that there are no conflicts of interest regarding the publication of this article.

REFERENCES

[1] Jafari E, Jarah-Najafabadi NT, Jahanian-Najafabadi A, Poorirani S, Hassanzadeh F, Sadeghian-Rizi S. Synthesis and evaluation of antimicrobial activity of cyclic imides derived from phthalic and succinic anhydrides. Res Pharm Sci, 2017; 12: 526-534.

[2] Ravasco JMJM, Faustino H, Trindade A, Gois PMP. Bioconjugation with Maleimides: A Useful Tool for Chemical Biology. Chemisrty A European Journal, 2019; 25: 43-59.

[3] Hamad AS, Abed FS. Synthesis of some new maleimide derivatives. Journal of Applicable Chemistry, 2014; 3: 56-63.

[4] Noldin VF, Locatelli C, Cordova CAS, Noldin AT, Vanzin F, Dajal fae J, Buzzi FC, Pilati C, Cechinel-Filho V, Creczynski-Pasa TB. Cytotoxicity of N-phenylmaleimide Derivatives and Inhibition of Melanoma Growth in a Preclinical Mouse Melanoma Model. Journal of Pharmacy and Pharmaceutical Sciences, 2015; 4: 32-42.

[5] Onimura K, Matsushima M, Yamabuki K, Oishi T. Synthesis and properties of N-substituted maleimides conjugated with 1,4-phenylene or 2,5-thienylene polymers. Polymer Journal, 2010; 42: 290-297.

[6] Al-Azzawi AM, Mahdi SA. Synthesis and evaluation of antimicrobial activity of several new maleimides to benzothiazole moiety. J Baghdad Sci, 2013; 10: 658-672.

[7] Dhivare RS, Rajput SS. Synthesis and antimicrobial activity of five membered cyclic imide derivatives of mono, di and tri substituted aromatic amines and napthyl amine. World J Pharm Res, 2015; 4: 1650-1658.

[8] Chin TS, Nasir FI, Hassan NI. Synthesis and antimicrobial activities of eleven N-substituted maleimide. Malaysian Journal of Analytical Sciences, 2016; 20: 741-750.

[9] Khalil AE, Berghot MA, Gouda MA. Synthesis and study of some new N-substituted imide derivatives as potential antibacterial agents. Chem Paper, 2010; 64: 637-644.

[10] Salhi L, Bouzroura-Aichouche S, Benmalek Y, Bentarzi Y, Poulain-Martini S, Cacciuttolo B, Dunach E, Nedjar-Kolli B. An efficient conversion of maleimide derivatives to 2-thioxo imidazolidinones. Organic Communications, 2013; 6: 87-94.

[11] Sortino M, Filho VC, Corre R, Zacchino S. N-Phenyl and N-phenylalkyl-maleimides acting against Candida spp.: Time-to-kill, stability, interaction with maleamic acids. Bioorg Med Chem, 2008; 16: 560-568.

[12] Stiz D, Corrêa R, D'Auria FD, Simonetti G, Cechinel-Filho V. Synthesis of cyclic imides (Methylphtalimides, carboxylic acid phtalimides and itaconimides) and evaluation of their antifungal potential. Med Chem, 2016; 12:647-654.

[13] Patil MM, Rajput SS. Succinimides: Synthesis, reaction, and biological activity. Int J Pharm Sci, 2014; 6:8-14.

[14] Xu G, Kong D, Li W, Xu W, Jiang Y. Synthesis of maleimide derivatives via CuAAC click chemistry and biological evaluation of their antitumor activity against cancer cell lines. Journal of Chemical and Pharmaceutical Research, 2014; 6: 947-951.

[15] Lee YJ, Huang CC, Lin WL, Hung CH. Camphorataimide B, a maleimide in mycelium of Antrodia camphorate, inhibits progression of human MDA-MB-231 breast cancer cells. Cancer Research Frontiers, 2016; 2: 43-54.

[16] Sahooa SK, Nagasree KP, Namratha JR, Varma PR, Kumar MMK. Synthesis and screening of new maleimide derivatives as potential anti-tubercular agents. Journal of Applied Pharmaceutical Science, 2015; 5: 44-47.

[17] de Campos F, Corrêa R, de Souza MM, Yunes RA, Nunes RJ, Cechinel-Filho V. Studies on new cyclic imides obtained from aminophenazone with analgesic properties. Potent effects of a 3,4-dichloromi derivative. Arzneimittelforschung, 2002; 52: 455-461.

[18] Huang P, Yeh YM, Pao CC, Chen CY, Wang TZC. N-(1-Pyrenyl) maleimide inhibits telomerase activity in a cell free system and induces apoptosis in Jurkat cells. Molecular Biology Reports, 2012; 39: 8899-8905.

[19] Gunosewoyo H, Midzak A, Gaisina IN, Sabath EV, Fedolak A, Hanania T, Brunner D, Papadopoulos V, Kozikowski AP. Characterization of Maleimide-Based Glycogen Synthase Kinase-3 (GSK-3) Inhibitors as Stimulators of Steroidogenesis. Journal of Medicinal Chemistry, 2013; 56: 5115-5129.

[20] Eloh K, Demurtas M, Mura MG, Deplano A, Onnis V, Sasanelli N, Maxia A, Caboni P. Potent Nematicidal Activity of Mi Derivatives on Meloidogyne incognita. Journal of Agricultural and Food Chemistry, 2016; 64:4876-4881.

[21] Imran M, Bisht AS, Asif MA. Review on Biological and Chemical Potential of Phthalimide and Maleimide Derivatives. Acta Scientific Pharmaceutical Sciences, 2019; 3: 51-67.

[22] Frisch MJ, Trucks GW, Schlegel HB et al. Gaussian 09, Revision B.01, Gaussian, Inc., Wallingford CT, 2010.

[23] Becke AD. A new mixing of Hartree-Fock and local density-functional theorie. J Chem Phys, 1993; 98: 1372-1377.

[24] Lee C, Yang W, Parr RG. Development of the Colle-Salvetti correlation-energy formula into a functional of the electron density. Phys Rev B, 1988; 37: 785-789.

[25] Zhao Y, Truhlar DG. The M06 suite of density functionals for main group thermochemistry, thermochemical kinetics, noncovalent interactions, excited states, and transition elements: two new functionals and systematic testing of four M06-class functionals and 12 other functionals. Theoretical Chemical Accounts, 2008; 120: 215-241.

[26] Dennington RI., Keith T, Millam J. GaussView, Version 5.0.8, Semichem. Inc., Shawnee Mission, KS, 2008.

[27] Jamroz MH.Vibrational Energy Distribution Analysis, VEDA4 program, Warsaw, 2004.

[28] Boys SF, Bernardi F. The calculation of small molecular interactions by the differences of separate total energies. Some procedures with reduced errors. Mol Phys, 1970; 19: 553-566.

[29] Nejad A, Suhm MA. Concerted Pair Motion Due to Double Hydrogen Bonding: The Formic Acid Dimer Case. J. Indian Inst Sci, 2019; 100: 15-19.

[30] Arı H, Pandır D, Böyükata M. Structural, energetics and vibrational analyses of monomeric and dimeric forms of 2-deoxy-2-(3-methyl-3-nitrosourea)-1-D-glucopyranose. Journal of Molecular Structure, 2021; 1229: 129588.

[31] Merrick JP, Moran D, Radom L. An Evaluation of Harmonic Vibrational Frequency Scale Factors. J Phys Chem A, 2007; 111: 11683-11700.

[32] Andersson MP, Uvdal P. New Scale Factors for Harmonic Vibrational Frequencies Using the B3LYP Density Functional Method with the Triple-ú Basis Set 6-311+G(d,p). J. Phys. Chem. A, 2005; 109: 2937-2941.

[33] Arı H, Özpozan T, Büyükmumcu Z, Akın N, İlhan İÖ. Synthesis, Spectral and Theoretical (DFT) Investigations of 4,6-diphenyl-6-hydroxy-1-{[(1Z)-1-phenyl ethylidene] amino} tetrahydro pyrimidine-2(1H)-one. Journal of Molecular Structure, 2022; 1250: 131820.

[34] Ünal Y, Nassif W, Özaydin BC, Sayin K. Scale factor database for the vibration frequencies calculated in M06-2X, one of the DFT methods. Vibrational Spectroscopy, 2021; 112: 103189.

[35] Kesharwani MK, Brauer B, Martin Jan ML. Frequency and Zero-Point Vibrational Energy Scale Factors for Double-Hybrid Density Functionals (and Other Selected Methods): Can Anharmonic Force Fields Be Avoided?. J Phys Chem A, 2015; 119: 1701-1714.

[36] Woldbaek T, Klaboe P, Nielsen CJ. The vibrational spectra of maleimide and N-D maleimide. J Mol Struct, 1975; 27: 283-301.

[37] Coates J. Interpretation of infrared spectra, a practical approach, in: R.A. Meyers (Ed.), Encyclopedia of Analytical Chemistry, John Wiley & Sons Ltd, Chichester, 2000.

[38] Katritzky AR. Infrared absorption of heteroaromatic and benzenoid sixmembered, monocyclic nuclei. Part V. The correlation of intensities of CC and CN ring stretching frequencies with charge disturbance in the ring. J Chem Soc, 1958.

[39] Arı H, Büyükmumcu Z, Özpozan T, İlhan Öİ, Bahadır Ö. Vibrational and Theoretical Analysis of Pentyl-4-benzoyl-1-[2.4-dinitrophenyl]-5-phenyl-1H-pyrazole-3-carboxylate. Spectrochimica Acta Part A: Molecular and Biomolecular Spectroscopy, 2013; 110: 193-204.

[40] Silverstein RM, Bassler GC, Morrill TC. Spectrometric Identification of Organic Compounds. 4th Edition, John Wiley and Sons, New York, 1981.

[41] Uesugi Y, Mizuno M, Shimojima A, Takahashi H. Transient Resonance Raman and ab Initio MO Calculation Studies of the Structures and Vibrational Assignments of the T_1 State and the Anion Radical of Coumarin and Its Isotopically Substituted Analogues. J Phys Chem, 1997;101: 268-274.

[42] Ramesh P, Caroline ML, Muthu S, Narayana B, Raja M, Geoffrey AB. Spectroscopic, chemical reactivity, molecular docking investigation and QSAR analyses of (2E)-1-(3-bromo-2-thienyl)-3-(2, 5-dimethoxyphenyl) prop-2-en-1-one, Spectrochim. Acta A Mol. Biomol. Spectrosc, 2019; 222: 117190.

[43] Parr RG, Pearson RG. Absolute hardness: companion parameter to absolute electronegativity, J Am Chem Soc, 1983; 105: 7512-7516.

[44] Domingo LR, Aurell MJ, Pérez P, Contreras R. Quantitative characterization of the global electrophilicity power of common diene/dienophile pairs in Diels-Alder reactions. Tetrahedron, 2002; 58: 4417-4423.

[45] Parthasarathi R, Subramanian V, Roy DR, Chattaraj PK. Electrophilicity index as a possible descriptor of biological activity, Bioorg Med Chem, 2014; 12: 5533-5543.

[46] Yang W, Mortier WJ. The use of global and local molecular parameters for the analysis of the gas-phase basicity of amines. J Am Chem Soc, 1986; 108: 5708-5711.

[47] Ayers PW, Parr RG. Variational Principles for Describing Chemical Reactions: The Fukui Function and Chemical Hardness Revisited. J Am Chem Soc, 2000; 122: 2010-2018.

[48] Ayers PW, Parr RG.Variational Principles for Describing Chemical Reac-tions. Reactivity Indices Based on the External Potential, Am Chem Soc, 2001; 123: 2007-2017.

[49] Morell C, Grand A, Toro-Labbé A. New dual descriptor for chemical reactivity. J Phys Chem A, 2005; 109: 205-212.

[50] Martínez-Araya J, Salgado-Morán G, Glossman-Mitnik D. Computational nanochemistry report on the oxicams conceptual DFT indices and chemical re-activity. J Phys Chem B, 2013; 117: 6339-6351.

[51] Cárdenas C, Rabi N, Ayers P, Morell C, Jaramillo P, Fuentealba P. Chemical reactivity descriptors for ambiphilic reagents: dual descriptor, local hyper-softness, and electrostatic potential. J Phys Chem A, 2009; 113: 8660-8667.

[52] Barluenga J, Tomas M, Bieger K. Reaction of Dihydrodiaza- phosphinines with Acetylenic Diesters: a Direct Synthesis of the λ5-Diazaphosphaazulene Skeleton, Eur J Org Chem, 1998; 7: 1425-1429.

[53] Correa JV, Herrera B, Toro-Labbe A. Characterization of the reactive conformations of protonated histamine through the reaction force analysis and the dual descriptor of chemical reactivity, Journal of Molecular Structure: Theochem, 2007; 817: 111-118.